Melt-cast microfibers of Cu-based shape memory alloy adopt a favorable texture for superelasticity

Citation: Tuncer, Nihan, and Christopher A. Schuh. "Melt-Cast Microfibers of Cu-Based Shape Memory Alloy Adopt a Favorable Texture for Superelasticity." Scripta Materialia 117 (May 2016): 46–50 © 2016 Elsevier Ltd

As Published: https://doi.org/10.1016/j.scriptamat.2016.02.011

Publisher: Elsevier

Persistent URL: http://hdl.handle.net/1721.1/115100

Version: Author's final manuscript: final author's manuscript post peer review, without publisher's formatting or copy editing

Melt-cast microfibers of Cu-based shape memory alloy adopt a favorable texture for superelasticity

Nihan Tuncer, Christopher A. Schuh

Department of Materials Science and Engineering, Massachusetts Institute of Technology, 77 Massachusetts Avenue, Cambridge, MA 02139, USA

Abstract

Continuous production of shape memory alloy (SMA) fibers and microfibers is a non-trivial task due to the challenges associated with their undeformed memory and, for many copper-based SMAs, brittleness in non-engineered forms. Here we demonstrate the direct continuous casting of super-meter-scale Cu-based SMA microfibers into a desirable oligocrystalline microstructure that is not brittle. The melt-casting process used here develops a favorable texture as well, leading to large superelastic strains (above 8 %), beyond what is typical for non-single-crystal SMAs.

Cu-based shape memory alloys (SMAs) generally perform poorly when they are polycrystalline, due to intergranular cracking associated with their high elastic anisotropy and transformation mismatch strains. However, the same brittle SMAs can exhibit excellent shape memory and superelasticity, as well as fatigue properties that approach those of single crystals, when they are produced in fine dimensions and with a specific grain microstructure: an oligocrystalline or "bamboo" grain structure where the grain boundaries lay almost perpendicular to the fiber axis, reducing relative grain boundary area [1,2]. These materials could be used in a number of novel applications, such as smart textiles, if they could be manufactured in large quantities via a continuous process.

The development of continuous fine fibers of Cu-based SMAs is, however, a nontrivial challenge in processing science. Fiber forming in the solid state is complicated by the brittleness of polycrystalline fibers in either the austenitic or martensitic states, and by the shape memory property itself, which at some temperatures would favor the unprocessed shape. Direct fiber casting and solidification from the melt, on the other hand, bypasses working in the solid state, and can lead to semi-finished products with highly tailorable sizes, surface topographies and cross-sectional geometries. Direct casting processes such as melt spinning, the "in-rotating-water spinning process" (INROWASP) and twin-roll casting are viewed as preferred manufacturing processes for SMAs, with the challenge being to develop those processes to effect the desirable oligocrystalline structure.

For non-SMA alloys, detailed analyses of INROWASP processing parameters on fiber quality and various morphological characteristics are available in the literature [3–8]. The processing parameters, specifically including the ejection pressure, nozzle size, wheel speed, and ejection temperature, operate collectively to produce a corresponding cast fiber diameter and

microstructure. Texture formation due to a growth selectivity in the [100] direction in melt spun ribbons [9] and INROWASP fibers [4] has also been reported.

None of the above processing studies pertains specifically to SMAs, and published efforts on direct casting of Cu-based SMAs are mostly limited to melt spinning of millimeter-wide ribbons [9–17], with the exception of a few reports on INROWASP round SMA fibers [3,18]. Almost all of these studies rely on the addition of grain refiners such as titanium, boron, zirconium and chromium to increase the strength of the cast alloy material. The resulting fine-grained fibers and ribbons generally show poor superelasticity, i.e. reversible strains below 2 % [19]. In light of the need for a coarse, oligocrystalline structure in SMAs, in the present study we explicitly avoid the use of grain refiners, and aim for a coarse as-cast structure. Whereas the Cu-Al-Ni family of SMAs is more widely studied, here we introduce Mn as well. Mn is known to prevent brittle γ phase (Cu_9Al_4) formation, enabling good superelasticity [20–22].

Bulk alloy pieces with a nominal composition of Cu-24Al-4.4Mn-3.6Ni (at%) were first prepared by induction melting of high purity elemental powders under argon. Several super-meter-long fibers of approximately 45-300 μm diameter were produced using the INROWASP process with a rotating drum fiber caster (PSI Ltd. England). Argon gas was first ejected onto the water surface for 30 seconds to create a blanket prior to melt ejection. The ejection temperature was measured by submerging an R-type thermocouple with a protective silica sheath into the quartz crucible. Ranges over which the processing parameters were varied in the experiments are given in Table 1. Some of the runs were recorded with a Casio EX-F1 model high speed camera (600 frames per second). Several qualitative processing science results emerged connecting the fiber diameter to the solidification microstructure and corresponding superelastic behavior, and this will be the focus of the present letter.

Diameter, composition and surface characteristics of the as-cast fibers were characterized with a scanning electron microscope (SEM, JEOL JSM-6610LV) equipped with an energy-dispersive spectrometer (EDS). We assessed solidification texture using cross sections of the melt-spun fibers in combination with electron backscatter Kikuchi diffraction (EBSD) on a FEI XL-30 scanning electron microscope. Transformation temperatures and superelasticity of the fibers were measured with a differential scanning calorimeter (DSC, TA Instruments Q1000) and a dynamical mechanical analyzer (DMA, TA Instruments Q800), respectively.

Table 1. Processing parameters used in spin casting of the fibers.

	Ejection pressure, P (Pa)	Nozzle radius, R_0 (m)	Ejection temperature, T (°C)	Rotating wheel speed, V_{wheel} (m/s)
Minimum	3×10^5	0.95×10^{-4}	1200	9.4
Maximum	4×10^5	1.25×10^{-4}	1300	10.2

Long fibers that were produced by systematically varying one variable at a time between the maximum and minimum values in Table 1 can be broadly classified in two groups based on their

morphology and brittleness. While the first group of fibers had circular cross sections with smooth solidification surfaces and exhibited superelasticity in the as-cast condition, the second group of fibers had somewhat elliptical cross sections, rough surfaces and obvious brittleness revealed by simple handling. Our high speed camera investigations revealed the mechanistic origins of these fiber types based on two distinct behaviors of the liquid metal jet: the second group of brittle fibers with elliptic cross sections were obtained when the liquid metal jet penetrated into the water, while the first group of round, superelastic fibers was formed in conditions where the jet bounced from the surface of the water rather than penetrating it.

Figure 1a shows this basic result, with the inset camera images capturing typical penetrating vs. bouncing behavior of the liquid metal jet. At larger fiber sizes, we observe the penetrating mode, and it is exclusively for the finer fibers that the bouncing mode is attained. The data in Fig. 1a show the practical outcome of the processing mode: the bouncing mode, which involves slower cooling due to the lack of intimate contact with the water, favors round fibers with larger grain sizes. The larger and flatter fibers that penetrated into the water formed smaller grains, presumably due to faster and omnidirectional cooling. In this figure the data on the x-axis represent the larger axis of the fiber cross sections, and thus the apparently larger fibers are actually more oblate in cross-section as well. Whereas the larger fibers have multiple grains across their cross-section, the finer fibers are of the bamboo oligocrystalline structure, with a single grain spanning their width.

A photograph showing the typical appearance of such continuously cast fibers is shown in Fig. 1b, emphasizing the length and volume of material typically produced. The inset SEM image illustrates the typical character of a fiber produced in “bouncing mode”, which has a relatively smooth surface, a round cross-section, and extreme flexibility as evidenced by the simple knot tied in this particular sample for illustration. Fig 1c shows the surface topography of a fiber produced in “bouncing mode”. A common observation in such fibers was that while one side of the fiber showed the dendritic structure, the other side was smooth and free of surface features.

Fig. 2 presents a more detailed look at fiber geometries and grain structures, including the as-cast surface topographies and cross sections parallel and perpendicular to the fiber axis, for fibers cast at various sizes. The dendritic surface structure seen in fiber A suggests free solidification, i.e., no contact between the fluid and any other surface was present to constrain the surface topography during solidification. Since these fibers were produced in the “bouncing mode”, we speculate that the smooth side may have been the location where solidification began, likely at the point of contact with the water; solidification then proceeded (in vapor) across the fiber and completed on the upper free surface, leaving the dendritic appearance there. Fig. 2 also shows that fibers produced in bouncing mode are characterized by long grains that fully span the fiber cross section, which is also consistent with a directional solidification process nucleated from one side of the fiber.

By contrast, fiber B, which was produced in the “penetrating mode” shows the absence of dendritic solidification surface structures, and instead exhibits grooved and rumpled surfaces with large, generally longitudinal features that appear all around the circumference of the fiber. These characteristics are consistent with solidification occurring from every surface of the fiber inward towards its center, as would be expected for a fiber plunged into water. These fibers are also

characterized by smaller grains, which is consistent with a higher cooling rate and a greater number of nucleation sites. The penetrating mode of processing also leads to more elliptical cross-sections, which we attribute to deformation in the semi-solid range when the fiber impacts the rigid casting wheel beneath the water surface and partially flattens.

The bouncing mode of processing is of great practical interest because of the bamboo grain structure seen in fiber A, and the utility of such oligocrystalline structures for shape memory and superelastic properties as described in the introduction. Interestingly, the tendency to form bamboo grain structures at smaller cast diameters has also been observed in INROWASP iron-silicon alloy fibers. Ichiryu et al. [23] observed long grains along the fiber axis in 70 μm filaments, whereas the grains were somewhat smaller in those with 130 μm diameter. They attributed this difference to the balance between the crystal growth rate and jet speed of the molten metal, resulting in an extreme anisotropy of crystal growth. At least in our experiments, we believe that achieving the bouncing mode of processing is critical to the formation of such oligocrystalline structures. This is borne out not only by our experimental observations with the high speed camera (cf. Fig. 1), but also by a simple Newtonian cooling analysis:

$$\frac{\Delta T(t)}{\Delta T(0)} = \exp\left(\frac{4th}{\rho D C_p}\right) \quad (1)$$

where $\Delta T(0) \sim 1300$ °C and $\Delta T(t)$ are the temperature difference between the alloy surface and the surroundings at the start of ejection (t=0) and time t, respectively, and $\rho = 7000\ kg/m^3$ and $Cp = 36.33\ Jmol^{-1}K^{-1}$ [24] are the density and heat capacity of the Cu alloy, respectively. Here h is an effective heat transfer coefficient for the cooling process, and while in principle this coefficient is a complex function of time as the fiber surface sees both vapor and then water contact (and then solid contact with the casting wheel), and experiences cooling both by radiation and convection, we may make a simple first order analysis by simply comparing solidification in vapor ($h \sim 10^2\ Wm^{-2}K^{-1}$) for "bouncing mode" and in agitated water ($h \sim 10^3 Wm^{-2}K^{-1}$) for "penetrating mode". For a fiber of D = 100 μm diameter, the cooling rate in penetrating mode ($\sim 10^4$ K/s), is about an order of magnitude higher than in bouncing mode ($\sim 10^3$ K/s). This large difference explains the much finer grains in the penetrating mode specimens, but it also supports our speculation that in the bouncing mode, crystallization begins at the contact point with the water where the heat extraction is momentarily very high relative to vapor-phase convection. The subsequent directional solidification across the fiber diameter under vapor convection conditions after losing contact with the water could form the bamboo grain structure.

As noted above, the bamboo structure achieved during "bouncing mode" processing is of practical importance for shape memory and superelasticity, and this is borne out by direct assessment of those properties. A typical result is shown for a single fiber of 100 μm diameter in Fig. 3a. For this specimen the transformation strain (ε_{tr}) between martensite start and finish was measured as 8.4 % by tensile testing at 20 °C, which is 45 °C above the austenite finish temperature measured by DSC. This is the highest experimentally-reported reversible strain of which we are aware in an as-cast non-single-crystalline Cu-based SMA, for which strains around 2 % are more common [25]. Higher superelastic strains in the range of 4-6 % were also reported on heat treated alloys and Taylor drawn fibers [1,2,22]. The present superelastic strain is more comparable to what is

attained in oriented single crystals or highly textured material prepared by cold rolling of sheets (~7%) [26] or cold-drawing and annealing of fibers (~ 9.2 %) [27]. The ability to continuously cast fiber that exhibits comparable superelasticity without any post manufacturing treatments is of practical interest.

Figure 3b shows the stress-assisted thermally induced transformation response of the same batch of fiber obtained by applying thermal cycles under constant external stress. The elongation upon cooling and subsequent contraction during heating increased with increasing external stress as expected. The onset of martensitic transformation in the thermal cycle with 97 MPa external stress is shown; an approximate transformation strain was measured as 8.2 %, which aligns well with the superelastic strain measured earlier at constant temperature.

Extending these kinds of measurements to a variety of fibers produced in the "bouncing mode", we observe a trend with respect to fiber diameter as shown in Fig. 3c. As the diameter of the cast fibers decreases, and as their relative grain size increases, the recoverable transformation strain increases. This suggests that solidification at finer scales produces a microstructure favorable to superelasticity. The fiber with very low relative grain size immediately broke before transformation, and is therefore represented as having zero transformation strain in the plot.

The desirable shape memory properties in Fig. 3, and their enhancement at finer fiber diameters, is, as described above, associated with the development of an oligocrystalline bamboo structure. However, the very high strains attained in these fibers also speak to a favorable crystallographic texture. Fig. 4 shows the grain orientation map obtained by EBSD on a longitudinal cross-section of a typical bouncing-mode fiber. This result was mirrored in a variety of other similar fibers that we studied as well, and here the inverse pole figure shows not only the typical grain orientations produced by the casting processing (in reference of the fiber axis), but also the theoretical axial transformation strains that Sutou et al. [26] calculated for a CuAlMnNi alloy. Our fibers generally consist of relatively few grains, all of which tend to be oriented close to the [001] and [101] directions, which are the favorable orientations in terms of transformation strains.

For a given fiber, we can approximate the expected transformation strain based on serial addition of the volume fractions of each grain, i.e. the theoretical strain of each orientation from Sutou et al. [26]. The locations of the individual grains are pointed in the theoretical inverse pole figure by color-coded circles in sizes proportional to their volume fraction. The theoretical strain approximated from this data is 8.5 %, which is very close to the measured value shown in Fig. 3a, and which supports the connection between processing-induced texture and the very high recoverable strains in these oligocrystalline SMAs.

In summary, we report a rapid and continuous processing method for Cu-based SMA fibers that exhibit single-crystal-like superelastic behavior with recoverable transformation strains above 8 %. These properties arise from the favorable microstructure inherent to the process, which nucleates large grains that grow across the fiber into an oligocrystalline structure, with a favorable crystallographic texture. The rapid, continuous production of such Cu-based SMA fibers with excellent superelastic and shape memory—with no post-processing required—speaks to an interesting possible manufacturing route for inexpensive smart fabrics and textiles.

Acknowledgements

This work was supported by the U. S. Army Research Laboratory and the U.S. Army Research Office through the Institute for Soldier Nanotechnologies, under contract number W911NF-13-D-0001.

References

[1] Y. Chen, C. A. Schuh, Size effects in shape memory alloy microwires, Acta Mater. 59 (2011) 537–553.

[2] S.M. Ueland, C.A. Schuh, Superelasticity and fatigue in oligocrystalline shape memory alloy microwires, Acta Mater. 60 (2012) 282–292.

[3] P. Ochin, A. Dezellus, P. Plaindoux, J. Pons, P. Vermaut, R. Portier, et al., Shape memory thin round wires produced by the in rotating water melt-spinning technique, Acta Mater. 54 (2006) 1877–1885.

[4] Y. Ono, T. Ichiryu, I. Ohnaka, I. Yamauchi, Production process of grain orientation-controlled Fe-6.5 mass% Si alloy fiber using spinning in gas atmosphere followed by winding in rotating liquid, J. Alloys Compd. 289 (1999) 277–284.

[5] J. Liu, L. Arnberg, S. Savage, On the mechanisms of formation of directly cast rapidly solidified wires, J. Mater. Sci. Lett. 8 (1989) 122–124.

[6] G. Frommeyer, J. Gnauk, W. Frech, S. Zeller, Shape Flow Casting and In-rotating-liquid-spinning Processes for the Continuous Production of Wires and of High-strength and Soft Magnetic Metallic Fibres, ISIJ Int. 46 (2006) 1858–1864.

[7] Y. Ono, I. Ohnaka, I. Yamauchi, Production of Cu-Mn-Al heusler alloy wire by the in-rotating-water-spinning process and its properties.pdf, J. Japanese Inst. Met. 51 (1987) 755–761.

[8] Y. Ono, T. Ichiryu, I. Ohnaka, I. Yamauchi, Spinning phenomena, structure and magnetic properties of Fe-6.5 mass% Si alloy fiber produced by the in-rotating-liquid-spinning process, J. Alloys Compd. 289 (1999) 220–227.

[9] S. Eucken, J. Hirsch, E. Hornbogen, Texture and Microstructure of Meltspun Shape Memory Alloys, Textures Microstruct. 8 (1988) 415–426.

[10] J. V. Wood, P.H. Shingu, The effect of processing conditions and subsequent heat treatment on the transformation behavior of some rapidly solidified copper-base shape memory alloys, Metall. Trans. A. 15 (1984) 471–480.

[11] J. Dutkiewicz, J. Morgiel, T. Czeppe, E. Cesari, Martensitic Transformation in CuAlMn and CuAlNi Melt Spun Ribbons, 7 (1997) 1–6.

[12] J. Malarría, C. Elgoyhen, P. Vermaut, P. Ochin, R. Portier, Shape memory properties of Cu-based thin tapes obtained by rapid solidification methods, Mater. Sci. Eng. A. 438-440 (2006) 763–767.

[13] G. Lojen, M. Gojić, I. Anžel, Continuously cast Cu–Al–Ni shape memory alloy – Properties in as-cast condition, J. Alloys Compd. 580 (2013) 497–505.

[14] H. Morawiec, J. Lelątko, D. Stróż, M. Gigla, Structure and properties of melt-spun Cu–

Al–Ni shape memory alloys, Mater. Sci. Eng. A. 273-275 (1999) 708–712.

[15] A.C. Kneissl, E. Unterweger, G. Lojen, Functional properties of wires and thin ribbons of several shape memory alloys, Adv. Eng. Mater. 8 (2006) 1113–1118.

[16] T. Goryczka, H. Morawiec, Texture and TWSM effect induced in Cu-Al-Ni melt-spun ribbons, Mater. Sci. Eng. A. 378 (2004) 248–252.

[17] G. a. Lara-Rodriguez, G. Gonzalez, H. Flores-Zúñiga, J. Cortés-Pérez, The effect of rapid solidification and grain size on the transformation temperatures of Cu-Al-Be melt spun alloys, Mater. Charact. 57 (2006) 154–159.

[18] S. Zeller, J. Gnauk, Shape memory behaviour of Cu–Al wires produced by horizontal in-rotating-liquid-spinning, Mater. Sci. Eng. A. 481-482 (2008) 562–566.

[19] P. Ochin, A. Dezellus, P. Plaindoux, J. Pons, P. Vermaut, R. Portier, et al., Shape memory thin round wires produced by the in rotating water melt-spinning technique, Acta Mater. 54 (2006) 1877–1885.

[20] M.A. Morris, Temperature and stress dependence of the shape memory effect produced by alloying additions in Cu-Al-Ni alloys, J. Phys. IV. 1 (1991) 335–340.

[21] C. Seguí, E. Cesari, Effect of Mn on Ageing of Cu-Al-Ni-Mn-B Alloys, Le J. Phys. IV. 05 (1995) C2–187–C2–191.

[22] M.A. Morris, T. Lipe, Microstructural influence of Mn additions on thermoelastic and pseudoelastic properties of Cu-Al-Ni alloys, Acta Metall. Mater. 42 (1994) 1583–1594.

[23] T. Ichiryu, Y. Ono, Ishihara, Structure and properties of melt-spun iron-silicon alloy filaments having single crystalline structure, J. Mater. Sci. 26 (1991) 1027–1031.

[24] and Y.V.G. Chekhovskoi, V. Ya, Valerii Dmitrievich Tarasov, Calorific properties of liquid copper, High Temp. 38 (2000) 394–399.

[25] K. Otsuka, C.M. Wayman, Shape memory materials, Cambridge University Press, London, 1999.

[26] Y. Sutou, T. Omori, R. Kainuma, N. Ono, K. Ishida, Enhancement of Superelasticity in Cu-Al-Mn-Ni Shape- Memory Alloys by Texture Control, 33 (2002).

[27] Y. Sutou, T. Omori, N. Koeda, R. Kainuma, K. Ishida, Effects of grain size and texture on damping properties of Cu–Al–Mn-based shape memory alloys, Mater. Sci. Eng. A. 438-440 (2006) 743–746.

[28] Y. Liu, D. Favier, L. Orgeas, Mechanistic simulation of thermomechanical behaviour of thermoelastic martensitic transformations in polycrystalline shape memory alloys, 115 (2004) 37–45.

FIGURE CAPTIONS

Figure 1. (a) During continuous casting, finer fiber diameters are associated with a transition from a "penetrating mode" where the fiber enters the water bed to a "bouncing mode" where the fiber bounces from the water surface and cools further in vapor. The grain size normalized to the fiber diameter rises at these finer scales. **(b)** Photograph showing strands of long, continuously cast fibers, with an inset SEM image illustrating the excellent flexibility of a 100 μm diameter fiber produced in bouncing mode, tied into a knot here for purposes of illustration. **(c)** An SEM image showing the surface topography of a fiber produced in "bouncing mode". These fibers are characterized by a smooth surface on one side and dendritic surface on the other.

Figure 2. Surface topography**,** cross sectional views parallel and perpendicular to the fiber axis of various fibers produced with different processing parameters. The fibers produced in "bouncing mode", e.g. Fiber A, tend to have round cross sections and the degree of oligocrystallinity improves with decreasing fiber diameter. The fibers processed in "penetrating mode", e.g. Fiber B, solidify into polycrystalline microstructures and have oblate cross-sections.

Figure 3. (a) Superelastic hysteresis response at 20 °C of a typical 100 micron fiber produced in "bouncing mode". Following the linear elastic region, the martensitic transformation starts at Ms forming a plateau and finishes at Mf where the stress starts to increase steeply. (b) Stress-assisted thermally-induced transformations measured on the same batch of wire under an external stress of 97 MPa show a similar degree of recoverable strain. (c) Variation of experimental transformation strains obtained by superelastic cycling for a variety of different fibers produced in "bouncing mode". The average relative grain size for each fiber is shown as data labels.

Figure 4. The orientation of the grains in a typical segment of an oligocrystalline cast fiber, with directions of the inverse pole figure presentation relative to the fiber axis reproduced from Ref. [26]. The locations of the individual grains are also denoted in the right inverse pole figure, color-coded and sized in proportion to the size of the grains. The contours in the right inverse pole figure show the theoretical axial transformation strain.

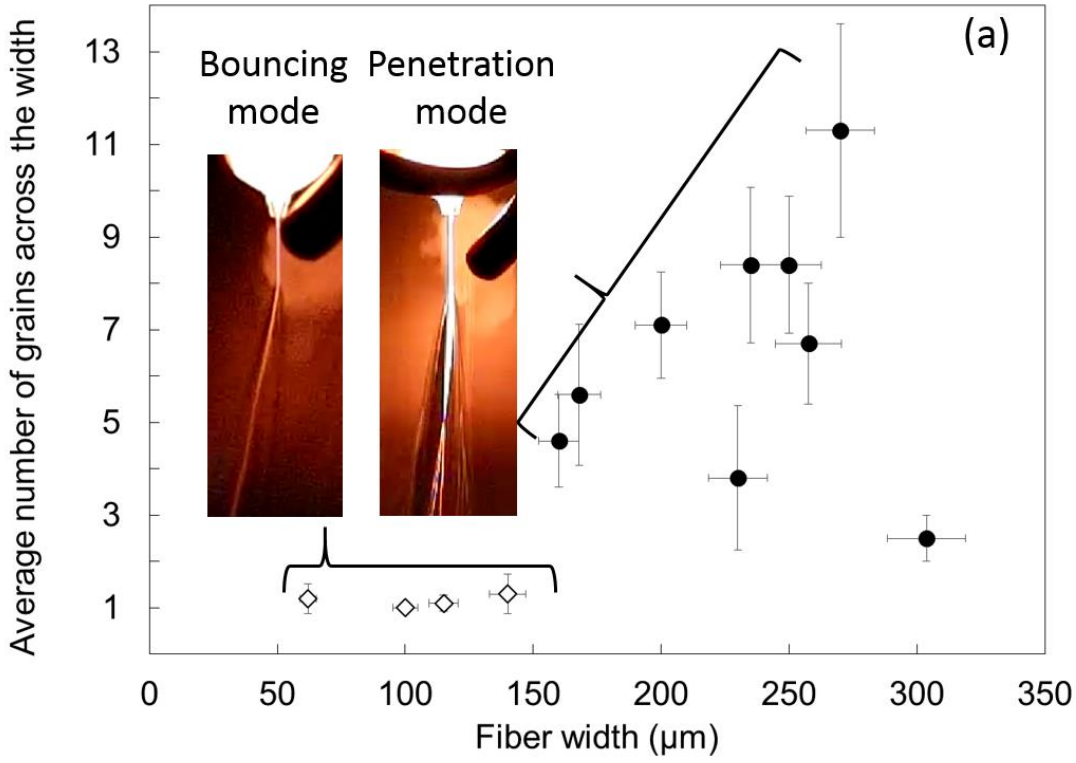
(a)
Bouncing mode
Penetration mode
Average number of grains across the width
13
11
9
7
5
3
1
0
50
100
150
200
250
300
350
Fiber width (μm)

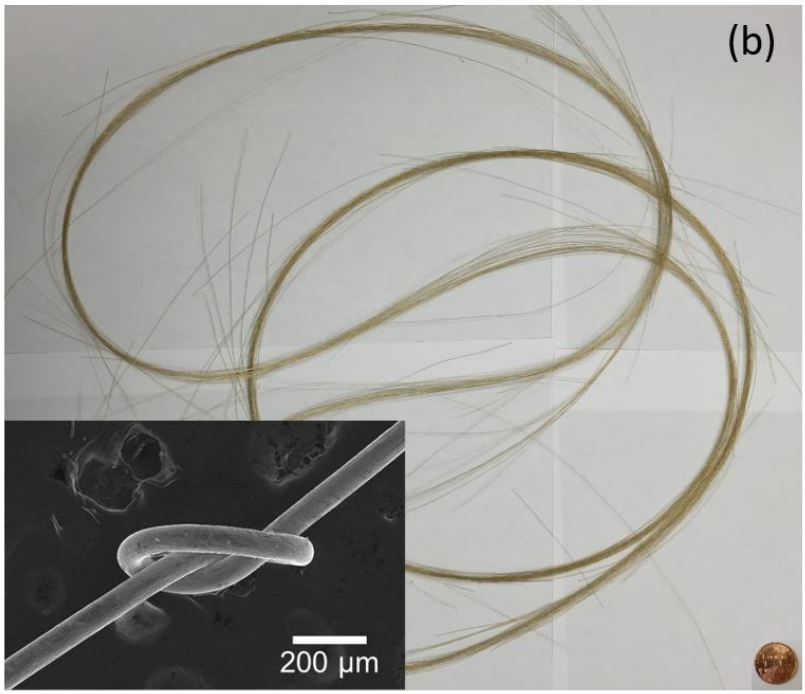
(b)
200 µm

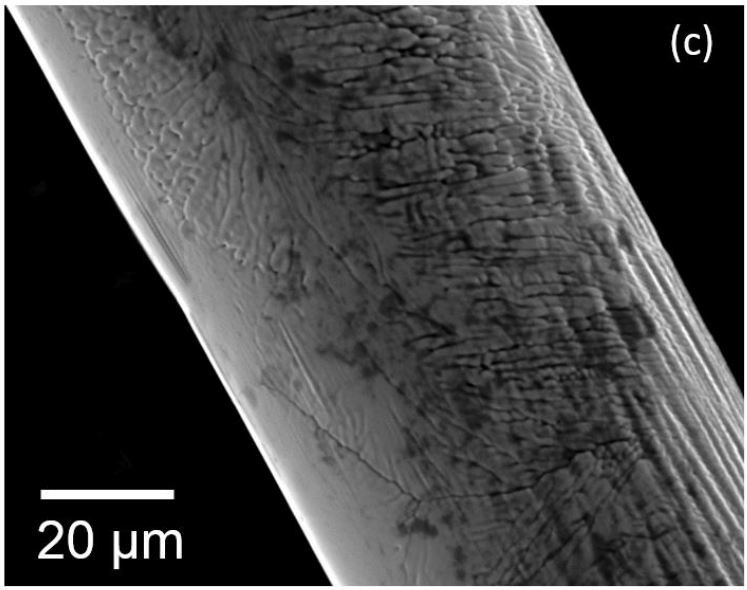

	Fiber surface	Longitudinal cross section	Axial cross section
Fiber A Long axis=140 µm Short axis=150 µm Bounced	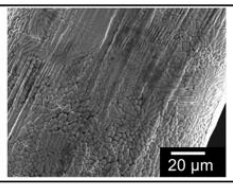	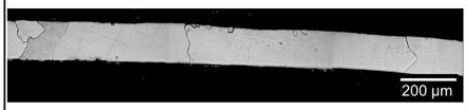	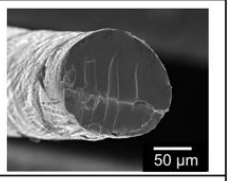
Fiber B Long axis~235 µm Short axis ~ 130 µm Penetrated	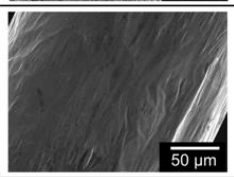		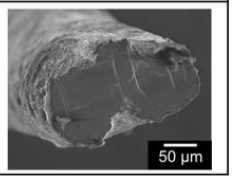

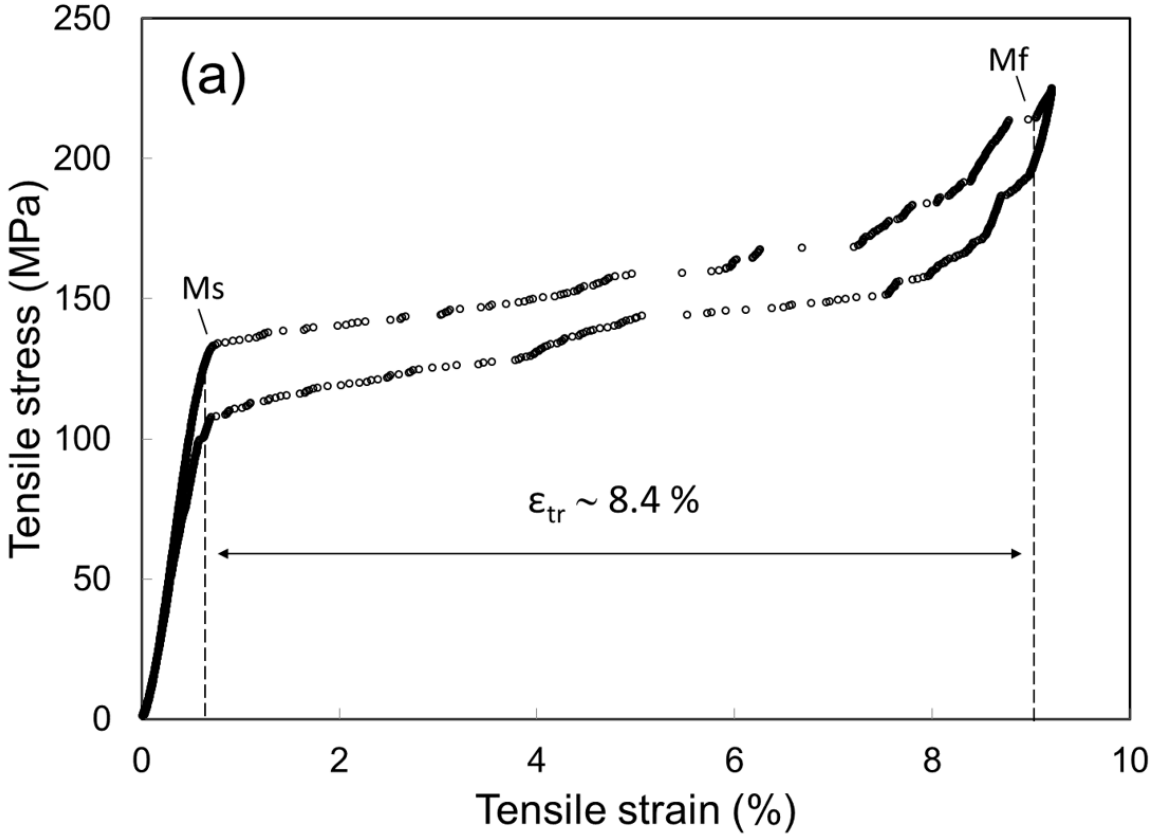
(a)
Mf
Ms
ε_{tr} ~ 8.4 %
Tensile stress (MPa)
Tensile strain (%)
250
200
150
100
50
0
0
2
4
6
8
10

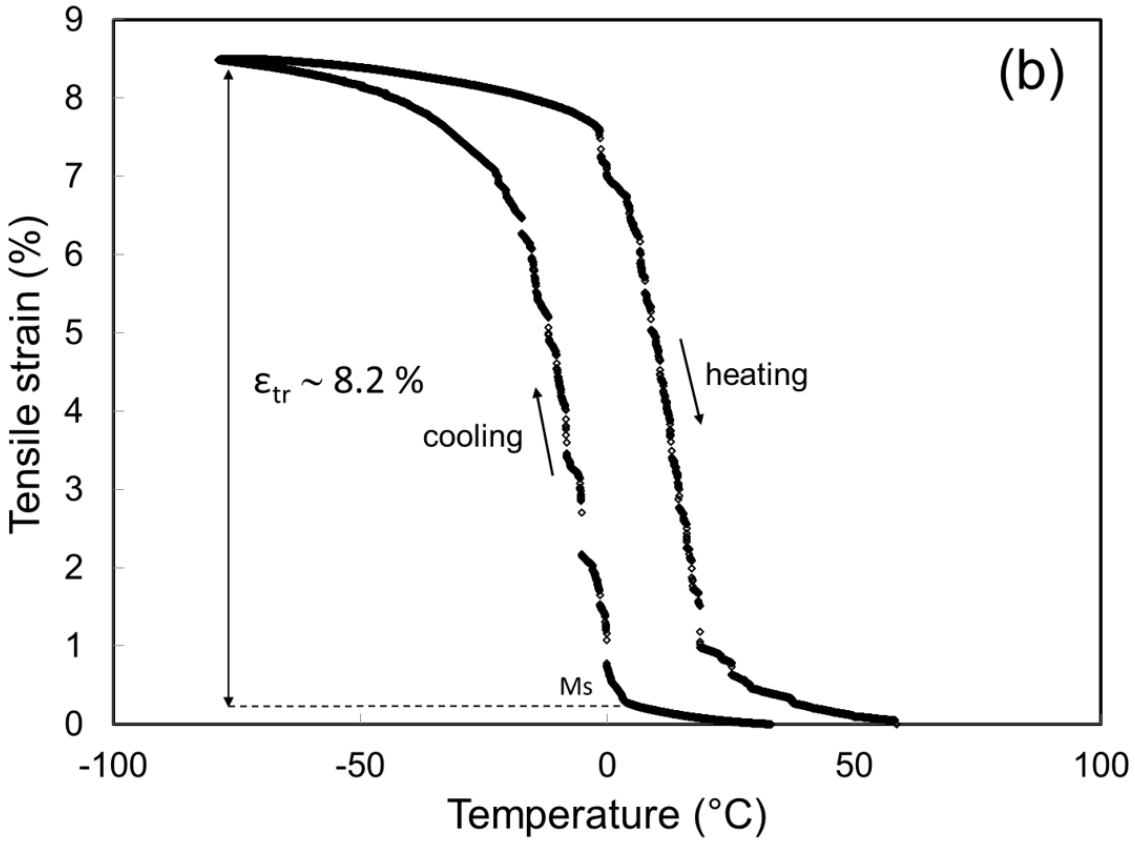
(b)
Tensile strain (%)
Temperature (°C)
ε_{tr} ~ 8.2 %
cooling
heating
Ms
9
8
7
6
5
4
3
2
1
0
-100
-50
0
50
100

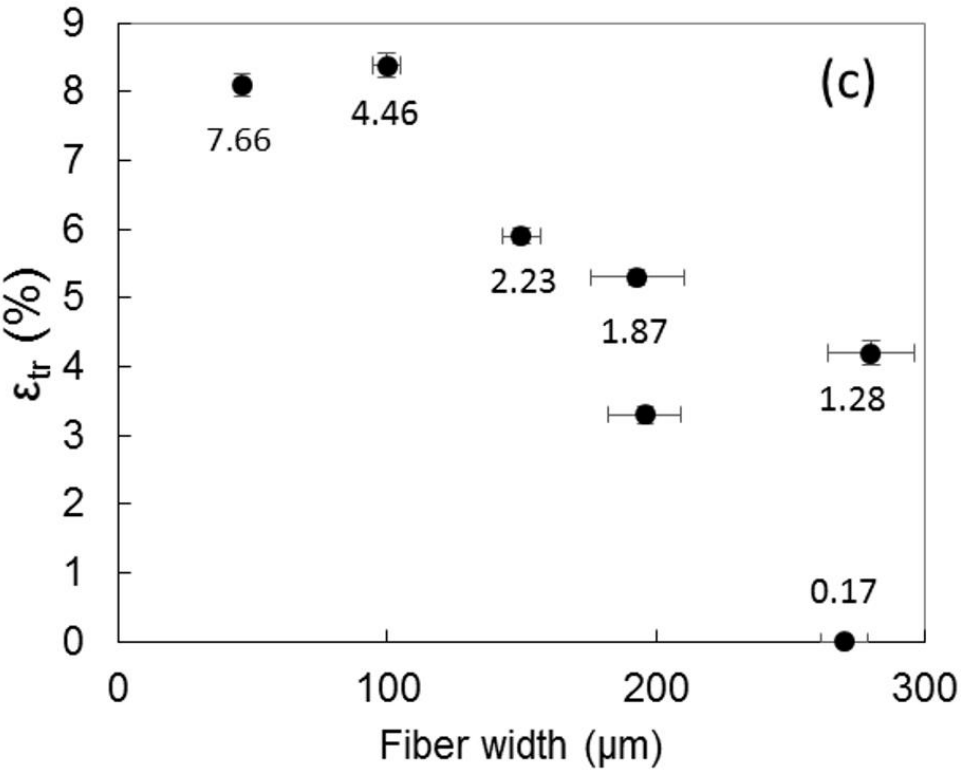
(c)
ε_{tr} (%)
Fiber width (μm)
7.66
4.46
2.23
1.87
1.28
0.17
0
100
200
300
1
2
3
4
5
6
7
8
9

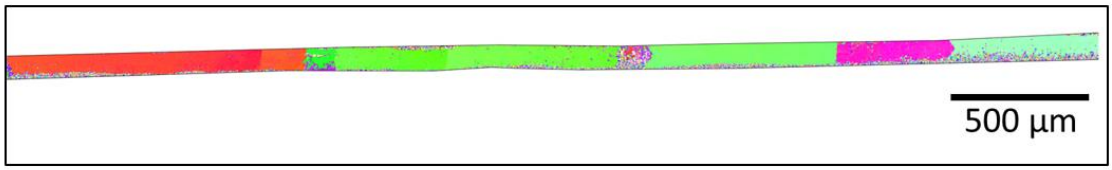
500 μm

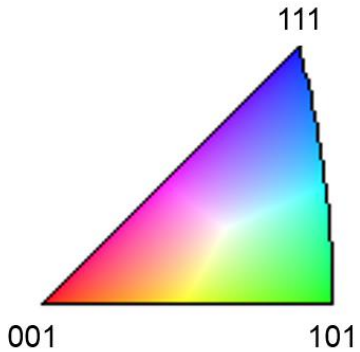
111
001
101

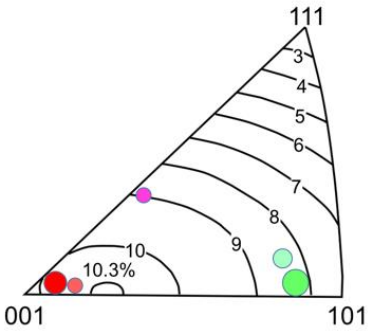
111
3
4
5
6
7
8
9
10
10.3%
001
101

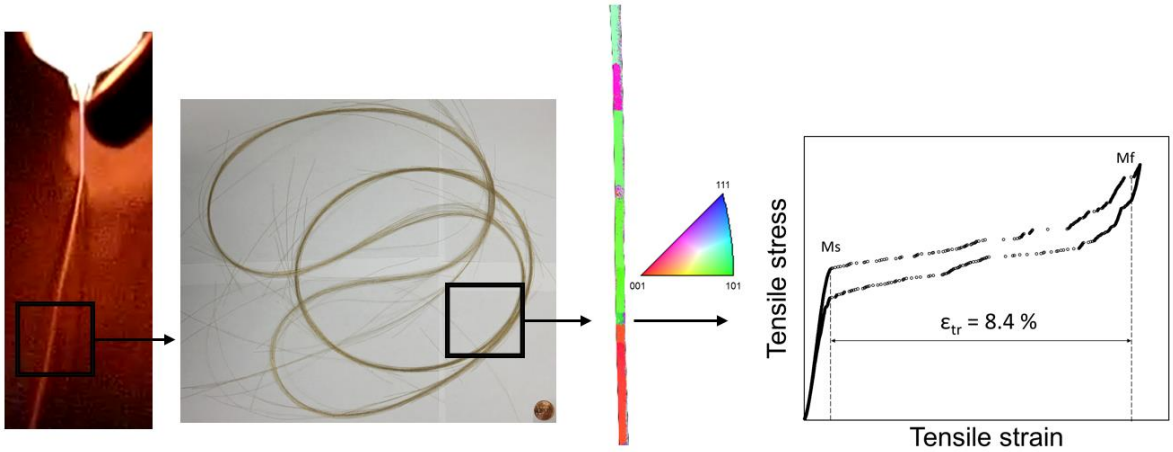
111
001
101
Mf
Ms
Tensile stress
ε_{tr} = 8.4 %
Tensile strain